A sustainable anode for Na-ion batteries based on holm oak waste-derived hard carbon and lignin binder

Received: 24 January 2025 | Revised: 28 February 2025 | Accepted: 25 March 2025

DOI: 10.1002/pc.29909

RESEARCH ARTICLE

Polymer COMPOSITES WILEY

Recycled milled carbon fibers in fused filament fabrication of composite filaments: Thermophysical analysis and 3D printability assessment for automotive parts manufacturing

Matteo Sambucci[1] | **Giovanna Colucci**[2] | **Luca Fontana**[2] | **Irene Bavasso**[1] | **Marco Valente**[1] | **Fabrizio Sarasini**[1] | **Massimo Messori**[2] | **Jacopo Tirillò**[1]

[1]Department of Chemical Engineering Materials Environment, Sapienza University of Rome and UdR INSTM, Rome, Italy

[2]Department of Applied Science and Technology (DISAT), Politecnico di Torino and UdR INSTM, Torino, Italy

Correspondence
Matteo Sambucci, Department of Chemical Engineering Materials Environment, Sapienza University of Rome and UdR INSTM, Via Eudossiana 18 00184, Rome, Italy.
Email: matteo.sambucci@uniroma1.it

Abstract

Recycled fibers like glass, carbon, and basalt are increasingly used in 3D-printed composites due to their high performance and sustainability. This study explores the use of recycled milled carbon fibers (rCFs) as fillers in polyamide-6,6 (PA66) filaments for automotive parts via fused filament fabrication (FFF). Building on prior research, the focus was on analyzing the rheological (melt mass flow rate) and thermal properties (thermogravimetry, differential scanning calorimetry, Vicat softening temperature) of PA66 filaments loaded with 5 and 10 wt% rCFs. Results showed that rCFs did not significantly affect the thermal stability of the PA66 matrix, with glass transition temperature and crystallinity remaining constant. A slight increase in melting and crystallization temperatures was observed, attributed to rCFs promoting nucleation and restricting molecular movement. The melt flow rate decreased with increasing rCF content, and the Vicat softening temperature increased by 3°C for 5 wt% rCF and 9°C for 10 wt% rCF. Then, prototypes of automotive shark fin antenna covers were 3D printed, showing good resolution and dimensional accuracy. However, structural defects could be improved by optimizing print parameters. Thermo-mechanical analysis showed no significant changes in thermal stability and transition temperatures. While minimal porosity (<4%) was observed, the Vicat softening temperature of the printed parts dropped by approximately 10°C, still within acceptable limits for automotive applications. Scanning electron microscopy images revealed slight defects such as air pockets and delamination but no fiber clustering.

Highlights

- rCFs are valid feedstocks for FFF and could be used for manufacturing automotive parts.

- Thermophysical investigation of PA-rCF filaments led to optimized 3D printing for component fabrication.
- The 3D printing process does not affect the thermal stability and characteristics of the composites.
- Optimizing printing parameters is crucial for improving the quality of printed parts.

KEYWORDS

automotive components, fused filament fabrication (FFF), PA6,6 filament, recycled carbon microfibers, thermophysical characterization

1 | INTRODUCTION

Three-dimensional printing technology involves advanced, customizable, and more sustainable fabrication methods compared to conventional manufacturing solutions. Considering some criteria including production costs, material costs, manufacturing time, energy inputs, recyclability, and labor patterns, reductions in CO_2 emissions and energy consumption of up to 5% by 2025 are estimated.[1] This aspect consolidates the role of additive manufacturing (AM) in the current industry. Fused filament fabrication (FFF), also known as fused deposition modeling (FDM), belongs to the extrusion-based 3D printing technologies and it is recognized as one of the most widespread AM methods both at the academic level and on an industrial scale (automotive, aerospace, medical, consumer goods) because of its low cost, low maintenance, high design flexibility, and capacity to create complex and functional geometries. FFF relies on depositing thermoplastic filaments layer by layer from a heated nozzle, which solidifies upon cooling to form the desired object, starting from a computer-aided design (CAD) 3D model.[1,2] Although 3D printing can be optimized through a careful selection of the process parameters, the characteristics of the filament material implemented in the process mainly govern the performance of the desired final object. In this regard, the addition of reinforcing fibers with optimal size and weight loading into the printable thermoplastic matrices is an established solution to enhance the properties of FFF printed parts.[3] The use of natural, mineral, or synthetic fillers not only reduces the cost of final products but also enhances the mechanical, thermal, and electrical properties, as well as their chemical and radiation stability, depending on the filler type and its intended functionality.[4]

The growing popularity of AM coincides with the growing attention to the sustainable development goals and environmental and resource protection, focusing attention on the development of innovative and eco-friendly 3D printable composites.[5] To meet these criteria, recent studies have been dedicated to developing more sustainable filaments by studying the possibility of integrating waste-derived thermoplastic matrices, including high-density polyethylene (HDPE), polylactic acid (PLA), polyethylene terephthalate (PET), polypropylene (PP), and acrylonitrile butadiene styrene (ABS),[6] as well as valorizing the use of recycled fillers and fibers.[7] In the last framework, the implementation of recycled carbon fibers (rCFs) has garnered remarkable attention over the past few years owing to their technological, environmental, and economic benefits, as well as to the massive potential waste generated from carbon fiber reinforced polymer composites.[8,9] While retaining excellent physical and mechanical properties comparable to virgin carbon fibers (vCFs), recent studies have demonstrated that the integration of rCFs has the potential to modify the mechanical strength, electrical conductivity, thermal conductivity, and wear resistance of 3D printed parts produced by FFF.[8] Su et al.[7] prepared and characterized rCFs reinforced polyamide-6 (PA6) filaments, investigating the influence of fiber dosage (up to 40 wt%) on the thermal and tensile properties of the 3D printed samples. The samples loaded with 20 and 30 wt% of rCFs showed the best mechanical performance. The tensile strength and elastic modulus of the optimal composite (20 wt% of rCFs) were improved by up to 175% and 329%, respectively, when compared with the unreinforced matrix and indicated a high degree of fiber alignment, relatively high degree of crystallinity, low fiber breakage, and low porosity (<6%). Liu et al.[10] mixed rCFs (10 wt%) with polyether-ether-ketone (PEEK) to produce composite filaments tailored for FFF printing. Tests on printed rCFs composite specimens featured an increase of 17% in the tensile strength compared to pure PEEK samples, an increase of 10% in the flexural strength, an increase of 97% in the electrical conductivity, an increase of 22% in heat conductivity (at 25°C), and a decrease in the friction coefficient and wear rate (11% and 75%, respectively), enabling higher engineering performance of 3D printed

parts. Fully recycled filaments produced from reclaimed post-consumer plastic matrix and waste fibers were investigated by Katalagarianakis et al.[11] The authors formulated and tested rCFs/recycled PET printable composites, evaluating the effect of fiber loading (from 0.4 up to 40.7 wt%) on the physico-chemical and mechanical properties of the printed parts. The tensile modulus improved by 390% for the highly loaded 40.5 wt% specimens. A fiber fraction of 40 wt% was found to be an upper limit considering fiber blockage in compounding and processability of the filament during printing. In addition, the presence of rCFs reduced the shrinkage up to 42% during printing compared to the unreinforced polymer.

Although the existing literature provides fairly complete background on the feasibility of using rCFs in thermoplastic filaments for FFF and on enhancing the engineering performance of printed specimens, none of the studies focused on the processability of these rCF-loaded composite filaments for the additive production of real-life industrial parts. Specifically, rCFs-based composites employed in automotive applications can provide great environmental and cost benefits compared to the manufacture with vCFs. Like virgin fibers, the reclaimed ones ensure a high strength-to-weight ratio, wear resistance, and good appearance. These peculiarities enable rCFs-based composites to be appealing materials for multiple applications in this sector.[9] Some companies, such as BMW Group,[12] Sanko Gosei UK,[13] and Racing Bulls S.P.A.,[14] have already implemented rCFs in some car components obtained via injection molding (rooftops, headlamps, instrument panels, flaps), boosting the potential viability and applicability of FFF 3D printing to the automotive industry.

This work presents an extension of a previously published research[15] dealing with the production and characterization of polyamide-6,6 (PA66)-matrix filaments for FFF 3D printing loaded with carbon microfibers, which were a byproduct of an industrial process for producing non-woven fabrics from pyrolyzed long fibers. This previous work also addressed the mechanical characterization of 3D printed composites, highlighting the need to conduct a wider investigation on the produced material to better understand the effect of the rCFs on the thermal and rheological behavior and to optimize their processability for FFF manufacturing. In the present study, the printability of PA66 filaments incorporated with 5 and 10 wt% of rCFs was optimized for the realization of 3D printed parts for the automotive industry. First, the filaments were subjected to thermo-rheological characterization, including thermogravimetric analysis (TGA), differential scanning calorimetry (DSC), melt mass flow rate (MFR) test, and Vicat softening temperature (VST) analysis to study the effect of the recycled milled fibers on the thermal stability and rheology of the filaments. These analyses served as a foundation for accurately defining the printing parameters used in the production of the prototype. Car shark fin antenna cover was chosen as a technological demonstrator to verify the feasibility of the filaments in the production of components for the automotive industry. Moreover, thermal and morphological analyses were then carried out on the printed specimens to verify the quality of the printing process and any alterations in thermo-mechanical behavior experienced by the material after the additive manufacturing processing.

2 | MATERIALS, EQUIPMENT, AND TESTING

2.1 | Raw materials

The base (matrix) material used for the FFF filaments production was a BASF Ultramid® 1000-11 NF2001 PA66 (BASF, Ludwigshafen, Germany). The selection of this thermoplastic matrix was driven by the widespread use of PA in the automotive industry due to several peculiarities, including mechanical strength, durability, thermal and chemical stability, abrasion resistance, and recyclability.[16] The rCFs used as reinforcement were provided by Carbon Task Srl (Biella, Italy). The fibers were recovered as a waste fraction from a patented industrial process converting pyrolyzed carbon fibers into non-woven fabrics (details in Ref. [15]). As a post-reclaiming stage, the rCFs were ball-milled into a powder form (Figure 1A) to achieve morphology suitable for filament extrusion. Scanning electron microscopy (SEM) on rCFs (Figure 1B), conducted by using a Tescan MIRA3 microscope (TESCAN, Brno, Czech Republic), revealed the coexistence of fibrous and powdery fractions resulting from the milling process to obtain the filler. Imaging-based size analysis on 90 individual fibers highlighted an average length of 30 ± 12 μm in accordance with the size distribution reported in Figure 1C.

The density of rCFs, determined with a helium pycnometer (AccuPycII 1340, MICROMERITICS, Norcross, GA, USA), was 1.917 ± 0.001 g/cm^3.

2.2 | Manufacturing of 3D printing composite filaments and properties

In this section, the fabrication process and physico-mechanical characterization of the filaments and 3D printed specimens are briefly described. The starting materials (PA66 and rCFs) were first dried in an oven at 80°C for 24 h and blended in different matrix/fibers ratios that is, 5 wt% of rCFs (PA-rCF5) and 10 wt%

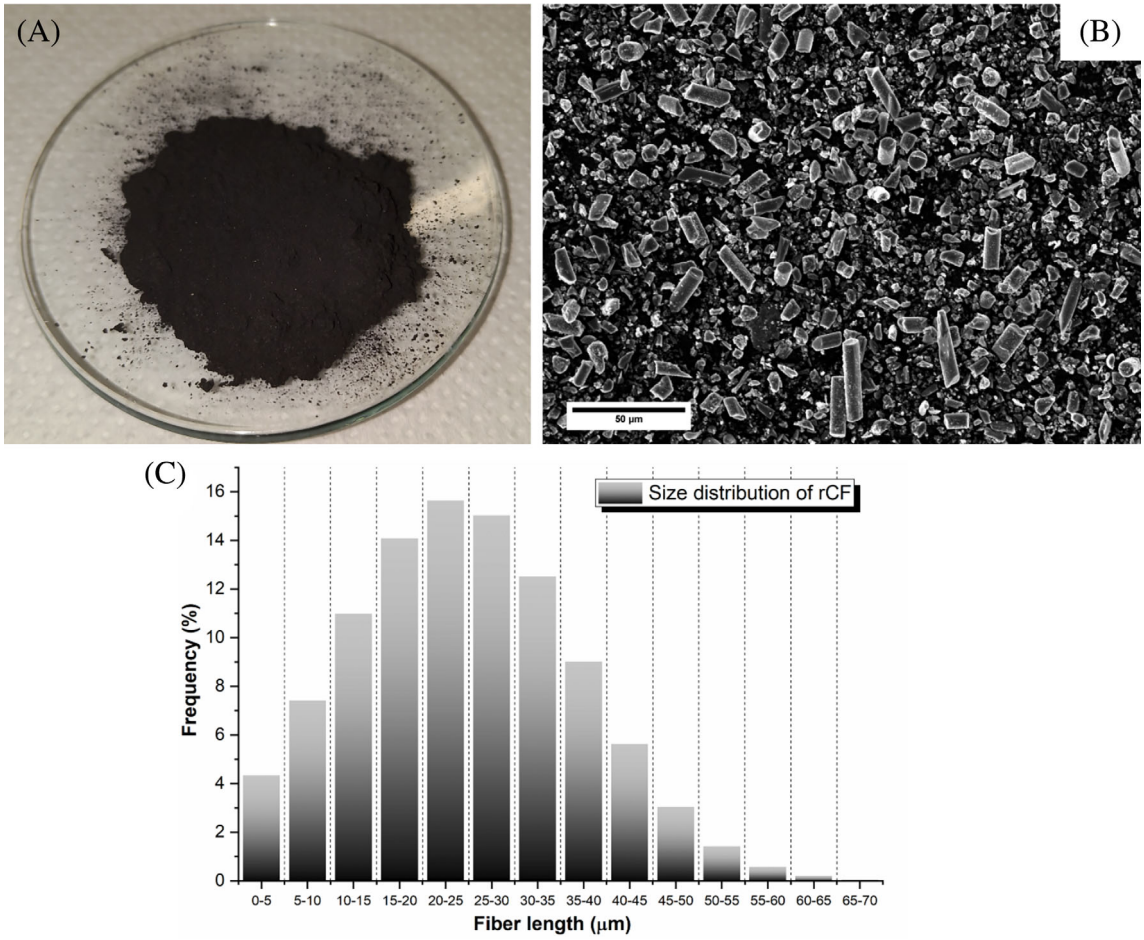

FIGURE 1 (A) Photograph of recycled milled carbon fibers (rCFs) used, (B) scanning electron microscopy (SEM) micrograph of rCFs, and (C) fiber size distribution.

(PA-rCF10). The compounds were then fed into a Thermo Scientific Process 11 twin-screw extruder (Thermo Fisher Scientific, Waltham, MA, USA) to produce the fiber-loaded filaments. Neat PA66 filament was also fabricated as a reference sample. Specific temperature profiles were implemented for unfilled and rCF-filled filaments. For neat PA66, the temperature profile in the eight heating zones was set as follows (from hopper to die): 255-255-260-260-260-255-250-235°C. For the composite filament, the temperature in each barrel zone was increased by 5°C to address the change in rheology induced by the addition of milled fibers. The screw speed was set at 150 rpm. Downstream of the die exit, the filament was cooled in air and pulled down by a roller positioned along the extrusion line, whose rotation velocity can be tuned to reach the desired diameter (1.75 mm). During the winding, the filament diameter was periodically checked by means of a digital caliper with a resolution of 0.01 mm to ensure the manufacturing of filaments with proper dimensional tolerance for a FFF 3D printing process (±0.05 mm).[17] More details on the filament manufacturing, including the tensile mechanical characterization of both composite filaments and 3D printed samples, are given in Reference [15]. The results of tensile tests on the composite filaments and standard dumbbell-shaped 3D printed specimens are tabulated in Table 1. These values serve as a reference for understanding the mechanical properties of the base composite material for the proposed industrial field. As discussed in Reference [15], the mechanical results showed that up to a certain rCF dosage (5 wt%), there is no significant deterioration of mechanical properties due to the filament processing via 3D printing. However, when the fiber content is increased to 10 wt%, a more pronounced loss of tensile properties in the printed samples is observed. This can be attributed to the increased extrusion complexity resulting from the rheological changes induced by the fillers, as well as the more pronounced frictional interaction between fibers, which causes a reduction in fiber length and weakens the reinforcing effect. Consequently, this prompted the present study to explore in depth the impact of rCF on the material's thermophysical

TABLE 1 Tensile properties of composite filaments and 3D printed samples from Reference [15].

Tensile test results: filament versus printed samples		
Sample	**Tensile strength (MPa)**	**Elastic modulus (GPa)**
PA-rCF5 (filament)	61.34 ± 1.52	2.37 ± 0.05
PA-rCF5 (printed)	61.74 ± 0.40	2.15 ± 0.02
PA-rCF10 (filament)	68.53 ± 3.04	2.58 ± 0.03
PA-rCF10 (printed)	59.53 ± 0.47	2.24 ± 0.01

properties, aiming to optimize its printability for real-life industrial applications.

2.3 | Material testing

2.3.1 | Thermo-gravimetrical analysis

TG measurements of the produced filaments and 3D printed composite samples were carried out by using a NETZSCH TG 209F1 Libra instrument (Netzsch, Selb, Germany) under nitrogen (N_2) gas with a flow rate of 40 mL/min from room temperature to 800°C with a heating rate of 10°C /min and a specimen weight of about 17 mg. The degradation temperatures and the real rCFs weight content (e.g., residue mass after the end of experiments) were obtained from the TG thermograms.

2.3.2 | Differential scanning calorimetry

DSC analysis was conducted, both on filament specimens and printed composites, using a DSC 214 Polyma by Netzsch (Netzsch, Selb, Germany). The specimens (~10 mg) were analyzed in a temperature range from −30 to 280°C implementing a heating/cooling/heating ramp of 10°C/min under N_2 atmosphere (60 mL/min). The results from the cooling and second heating scans were used to determine the thermal properties of tested materials, including the glass transition temperature (T_g), melting temperature (T_m), and crystallization temperature (T_c). The degree of crystallinity (X_c) of the polymer matrix was calculated in accordance with the following equation (Equation 1):

$$X_c(\%) = \frac{\Delta H_m}{\Delta H_m^0 \times (1 - w_f)} \times 100\%, \quad (1)$$

where ΔH_m refers to the melting enthalpy determined from the DSC curve, ΔH_m^0 is the melting enthalpy of the 100% crystalline PA 66 matrix $(\Delta H_m^0 = 196\,J/g)$,[18] and w_f is the weight fraction of rCFs.

2.3.3 | Melt mass flow rate

The melt flow properties of the filaments were studied in terms of MFR values by using an extrusion plastometer device (Mflow, Zwick/Roell, Ulm, Germany). First, each filament was pelletized by a blade shredder (Shredder 750, Felfil s.r.l., Turin, Italy). The pellets were dried in an oven at 80°C for 24 h to remove moisture before testing. Then, the plastometer barrel was fed with about 7 g of material. The test was carried out at 250°C with a nominal load of 5 kg, following the procedure outlined in the ISO 1133 standard method. The MFR results are reported as the mean value of five repetitions, including standard deviation.

2.3.4 | VST analysis

VST represents the temperature at which a flat-ended steel needle of 1 mm^2 circular cross section penetrates the specimen to a depth of 1 mm under a standard load of 10 N applied perpendicular to the test specimen. To assess the influence of the rCFs addition and any variation in VST following 3D printing, rectangular test specimens (length of 50 mm, width of 10 mm, and thickness of 2 mm) were produced from the filaments both by injection molding ($T_{cylinder} = 260°C - T_{mold} = 80°C$) and FFF, implementing the printing parameters optimized in the present work. The test (ISO 306 and ASTM D 1525) was conducted with a Amsler HDT/VICAT Allround (Zwick/Roell, Ulm, Germany) apparatus using silicone oil as an immersion bath, a temperature rate of 120°C/h, and a temperature range between 30 and 150°C. The tests were performed in duplicates.

2.3.5 | Porosity evaluation on printed samples

The influence that printing parameters have on the printed parts porosity is noteworthy. If the process is not properly optimized, it leads to the generation of inter-filament voids, which can be detrimental to the structural and durability performance of the additively manufactured component. The porosity percentage (%P) was evaluated on 3D printed composite specimens (PA-rCF5 and PA-rCF10) produced with 100% infill, considering the printing parameters reported in Table 2. The type of test specimens was the same as used in VST testing.

Equation (2), from Xiao et al.,[19] was used to calculate the %P value. The formula assumes that the filaments produced by extrusion were of negligible porosity.

$$P(\%) = \frac{(\rho_{fil} - \rho_{3D})}{\rho_{fil}} \times 100\%. \quad (2)$$

To measure the density of the filaments (ρ_{fil}) and printed specimens (ρ_{3D}), a water-displacement method was employed by means of a commercial density determination kit of the analytical balance Mettler Toledo ME54 (Mettler Toledo, Columbus, OH, USA). The ρ_{fil}-value was the average of 20 measurements taken on filament specimens of 30 mm length. The ρ_{3D}-value was computed on three printed specimens.

2.3.6 | Scanning electronic microscopy

The morphology of the 3D printed specimens was investigated by using a Phenom™ XL G2 Desktop Scanning Electron Microscope (Thermo Fisher Scientific, Waltham, Massachusetts, USA) at an accelerating voltage of 15 kV. Each specimen was previously fractured in liquid nitrogen, and the fracture surface was analyzed after metallization with platinum.

2.4 | Three-dimensional printing: design, modeling, and fabrication of the automotive demonstrators

To process the PA66 filament reinforced with recycled carbon fibers to realize the car shark fin antenna cover replica, a 3ntr A4V4 FDM machine (Jdeal-Form s.r.l, Oleggio, Novara, Italy) was used with a maximum hot end temperature of 450°C, as reported in Figure 2A. For the slicing process, *KISSlicer* PRO v1.6.3 Software was used, and the optimal printing parameters were found through its tune wizard in terms of hot end temperature, flow rate, preload, and destring.

In our case, the temperatures employed were found through the tuning wizard in line with the suggestion by Valente et al.[15]: 265°C for the PA-rCF5, and 270°C for the PA-rCF10 samples, respectively. The flow rate was set as a minimum value of 2.08 mm^3/s and a maximum value of 4.00 mm^3/s for PA-rCF5s, while a minimum value of 2.8 mm^3/s and a maximum value of 4 mm^3/s for PA-rCF10. The preload was set at 0.031 μs for PA-rCF5 and 0.028 μs for PA-rCF10. Tuning destring means reducing the slime during printing and reducing the aesthetic defects that can occur. For this reason, three pillars are printed to see how many aesthetic defects are made during the printing process. Destring values of 5 mm were set for both PA-rCF5 and PA-rCF10 samples.

After that, the bed temperature, necessary to assure that material adheres to the building plate during the print realization, was set at 90°C for the part produced with PA-rCF5. While for the part produced with PA-rCF10, the bed temperature was set at 110°C, as suggested by the paper mentioned before.[15] The chamber temperature was set at room temperature.

The 3D printed samples of the shark fin antenna covers were produced in two different sizes and infill percentages, a replica of the antenna with 25% infill, and a second hollow replica with 0% infill, twice as big as the one before. Figure 2 also shows the antenna shark fin replica with 25% (B) and 0% (C) infill in the *KISSlicer* environment.

The layer height used for the entire production was 0.2 mm. The 25% infill replica print was finally realized by 192 layers, while the hollow one sample was made by 396 layers of composite deposition. Moreover, the time requested to produce the 25% infill replica was about 1 h and 15 min, while the production of the hollow replica required about 2 h and 20 min. The main printing parameters used for the realization of the 3D printed parts were listed and summarized in Table 2.

3 | RESULTS AND DISCUSSION

3.1 | Thermal and rheological characterization of the 3D printed composite filaments

3.1.1 | Thermogravimetric analysis

The weight loss profile and the derivative thermogravimetric analysis (DTG) curves are reported in Figure 3A,B, respectively. Except for a slight initial mass loss between 100 and 200°C due to the evaporation of residual moisture, all samples showed a similar thermal-degradation behavior, resulting in a single-stage weight loss above 450°C. Neat PA66 filament underwent full degradation, displaying a maximum degradation temperature (T_{deg}) of 458°C. Several degradation mechanisms for PA66 have been proposed.[20] The first involves a homolytic cleavage of the peptide bond (CO-NH). The second pathway includes cis-elimination, leading to the breaking of the CH_2-NH bond. Additionally, depolymerization of PA66 into cyclic monomers has been suggested through a back-biting reaction or a radical recombination reaction. Thermograms of composite filaments showed residual mass indicating the presence of rCFs. In addition to T_{deg}, TGA results (Table 3) were also correlated to the decomposition temperatures $T_{5\%}$

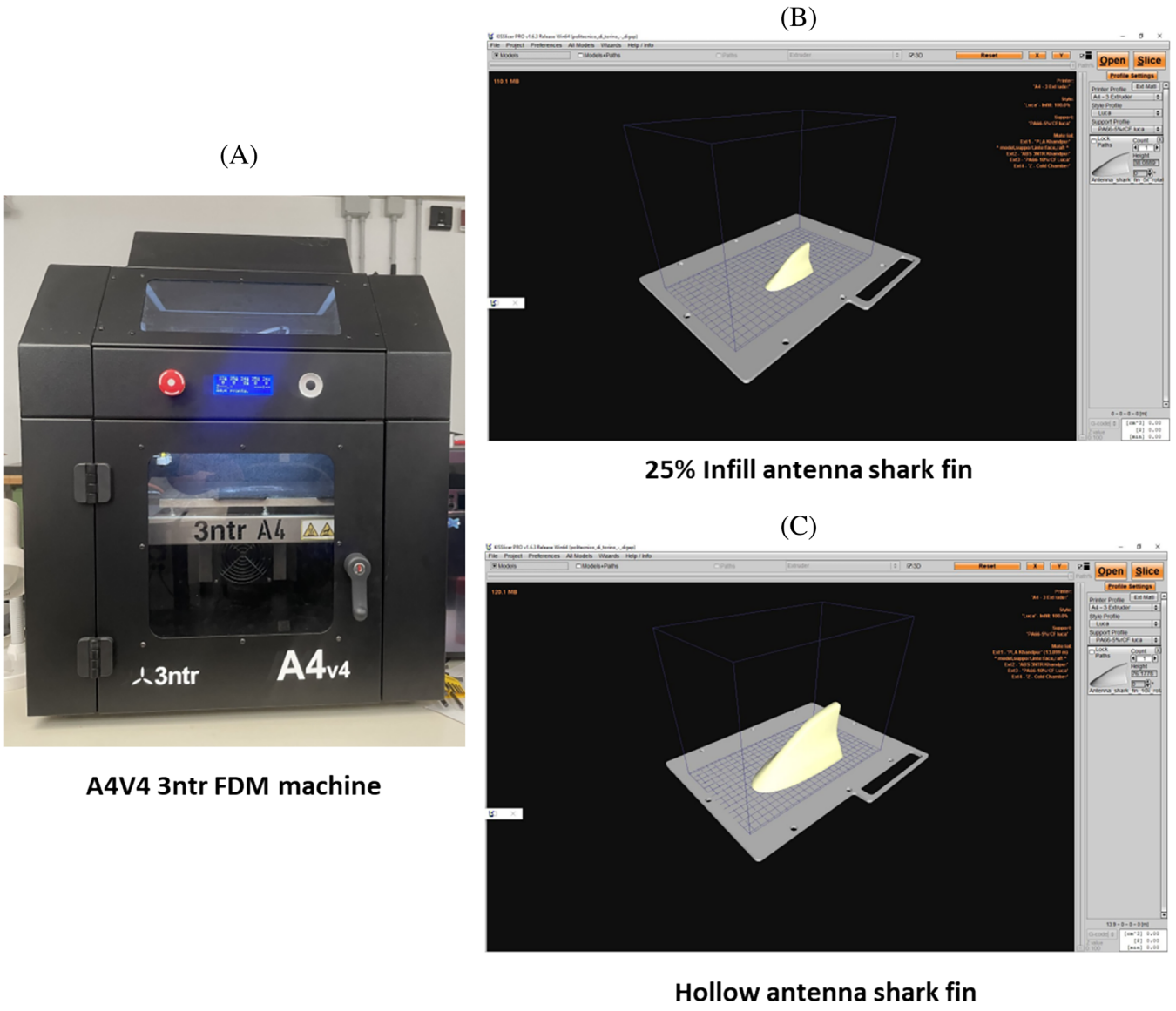

FIGURE 2 The A4V4 3ntr fused deposition modeling (FDM) machine (A) and the shark fin antenna cover replica with 25% (B) and 0% (C) of infill in the *KISSlicer* environment, respectively.

TABLE 2 Main printing parameters used during the 3D printing process of the antenna shark fins.

	Sample	
Parameter	**PA-rCF5**	**PA-rCF10**
Hot end temperature (°C)	265	270
Bed temperature (°C)	90	110
Chamber temperature (°C)	25	25
Layer height (mm)	0.2	0.2
Infill (%)	0/25	0/25
X/Y infill orientation (°)	+45/−45	+45/−45
Flow rate (min–max) (mm^3/s)	2.08–4.00	2.08–4.00
Destring (mm)	5	5
Preload (μs)	0.031	0.028

(i.e., temperature for 5% weight loss) and $T_{10\%}$ (i.e., temperature for 10% weight loss). Based on the reported data, two major outcomes can be drawn. Firstly, the concentration of rCFs incorporated into the composites did not significantly affect the thermal stability of the PA66 matrix. Other researchers[21,22] have found a slight increment in thermal stability of 3D printing filaments following the addition of milled carbon fibers due to the high thermal conductivity of carbon fillers, which facilitates the heat dissipation into the composite, delaying the thermal decomposition mechanism.[22] However, in the above-mentioned paper, this behavior was obtained considering carbon fiber levels higher than the one investigated in the present manuscript (i.e., >10 wt%). Secondly, the effective rCFs present in the filament were

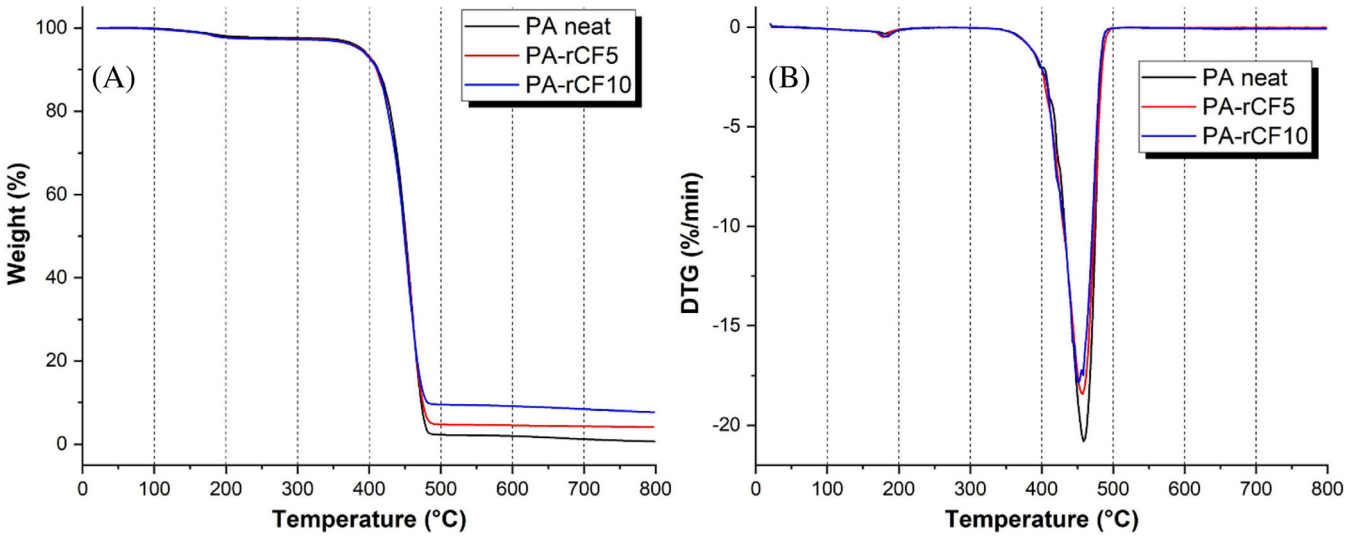

FIGURE 3 (A) Weight loss profile and (B) derivative thermogravimetric analysis (DTG) of neat polyamide (PA) and composite filaments.

TABLE 3 Results of thermogravimetric (TG) analysis on filament specimens.

TGA results of filaments				
Sample	$T_{5\%}$ (°C)	$T_{10\%}$ (°C)	T_{deg} (°C)	**rCFs content (%)**
PA neat	388	411	458	–
PA-rCF5	387	410	457	4.1
PA-rCF10	386	411	458	7.7

slightly lower than the input loadings, with a noticeable discrepancy (about 2.3%) in the case of the composite filament with the highest filler content (PA-rCF10). Although TGA requires multiple tests on the material to obtain an accurate evaluation regarding the homogeneity of the filament in terms of fiber content, this result can be primarily ascribed to the extrusion process, which can lead to a non-optimal homogeneity of the realized filaments in terms of the distribution of rCFs. It is clear that a better distribution of rCFs can be obtained by implementing a longer mixing time. The extension in processing time is a difficult task, which might lead to the degradation and downsizing of the fibers, limiting their effect on the mechanical properties of the composite.[23] However, the use of a powdery carbon fraction (such as the rCF used in this work) is less significantly affected by length reduction phenomena, making it possible to optimize the compounding process without excessively degrading the mechanical properties of the final material by devaluing the contribution of fiber reinforcement.

3.1.2 | Differential scanning calorimetry

Figure 4 illustrates the DSC curves of pure PA and the rCF-filled composite filaments. The T_g and X_c values were practically unaffected by the incorporation of milled fibers, with values of approximately 50°C and 28%, respectively, and the effect is not significantly influenced by the change in fiber concentration. Similar findings were found by Giani et al.,[21] who investigated the influence of rCFs addition (5 and 10 wt%) on the thermal and mechanical properties of PLA-matrix 3D printing filament. However, a slight effect following the addition of rCFs was detected in terms of melting and crystallization behavior. The values of T_m and T_c slightly increased from 178 to 180°C and from 142 to 145°C, respectively. The increment in melting point is induced by the effect of milled fibers to hinder the expansion and free movement of macromolecular chains. Therefore, macromolecular mobility is shifted towards higher temperatures, leading to an increase in T_m.[24] Concerning the crystallization behavior, T_c moved to higher temperatures due to the contribution of rCFs on the heterogeneous nucleation (establishment of nucleation sites), promoting the crystallization of the composite system, enabling the PA-matrix to start crystallization at a higher temperature.[24]

The corresponding thermal parameters are listed in Table 4.

In conclusion, it can be deduced that the implementation of this type and percentage of carbon fibers does not significantly alter the thermal properties of the polymer, while ensuring fair improvements in mechanical performance, as reported by the authors in

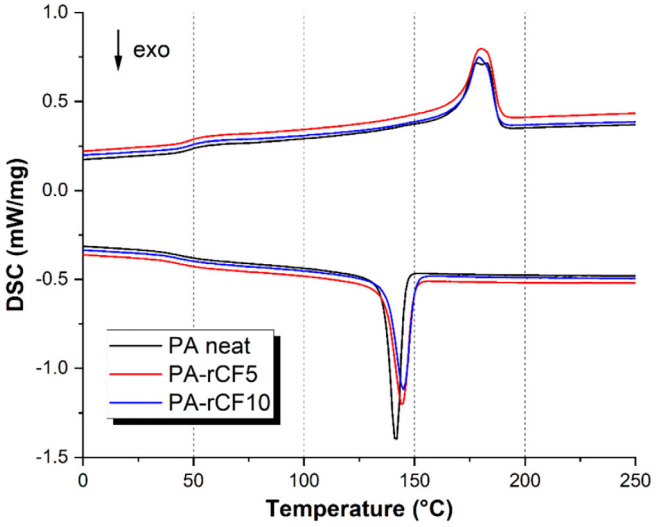

FIGURE 4 Differential scanning calorimetry curves of neat polyamide (PA) and composite filaments.

TABLE 4 Results of differential scanning calorimetry (DSC) measurements on filament specimens.

DSC results of filaments					
Sample	T_g (°C)	T_c (°C)	T_m (°C)	ΔH_m (J/g)	X_c (%)
PA neat	48	142	178	55.1	28
PA-rCF5	49	144	180	53.9	28
PA-rCF10	49	145	179	50.7	28

their previous research.[15] This aspect can be beneficial in terms of industrial scalability since it would allow integrating the developed materials into consolidated production lines without requiring expensive and energy-intensive changes in the process parameters.

3.1.3 | MFR test

Melt flow behavior of polymeric filaments for FFF is a crucial parameter for a successful printing process, as it can affect the extrusion quality as well as the accuracy and interlayer bonding of the printed part. Increasing the viscosity of the material, due to the addition of fibers within the polymeric matrix, results in structural defects including "non-printing", low interlayer adhesion, or nozzle clogging in 3D printers. Moreover, assessment of the flow behavior is strictly necessary for the selection of the proper printing parameters.[25,26]

MFR values of PA and rCF-filled filaments are shown in Figure 5. As expected, after the incorporation of the recycled carbon microfibers, the MFR of the PA-rCFs composites gradually decreased with the increase in rCFs content. With respect to the unfilled *PA* filament (MFR = 34 g/10 min), the MFR was reduced by 15% and 39% in the composites loaded with 5 and 10 wt% of rCFs, respectively. The presence of fibers negatively influences polymer rheology, causing a loss in the melt flow capability.[27] This drop in melt fluidity due to the incorporation of rCFs was compensated during the extrusion for filament manufacturing by increasing the temperature profile by about 5°C. The achieved MFR results will be used to set properly the 3D printing parameters with the aim of optimizing the processing and the quality of the printed part.

3.1.4 | VST analysis

VST provides information on the thermo-mechanical stability of polymers and composites, representing a valuable parameter for quality control, development, and characterization of polymeric materials, and it is generally adopted to establish the service temperature of thermoplastic polymers in industry.[28] An increment in VST can be verified following the addition of rCFs (Figure 6). VST increased by 3 and 9°C, respectively, when 5 and 10 wt% of rCFs were incorporated. In addition to the intrinsic thermal stability of milled carbon fibers, the presence of this filler restricted the motion of macromolecular chains, effectively improving the materials' stiffness under elevated temperatures. This effect resulted in the improvement of thermomechanical performance that can be crucial in materials selection for several polymer engineering applications to understand their thermal limits of service.[29]

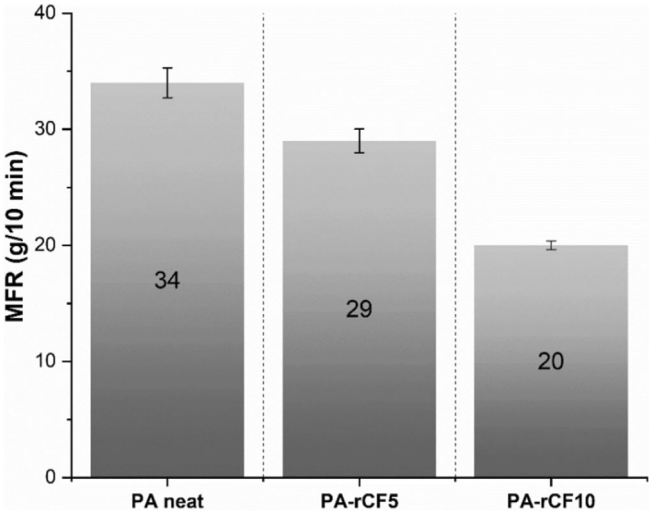

FIGURE 5 Melt mass flow rate (MFR) test results.

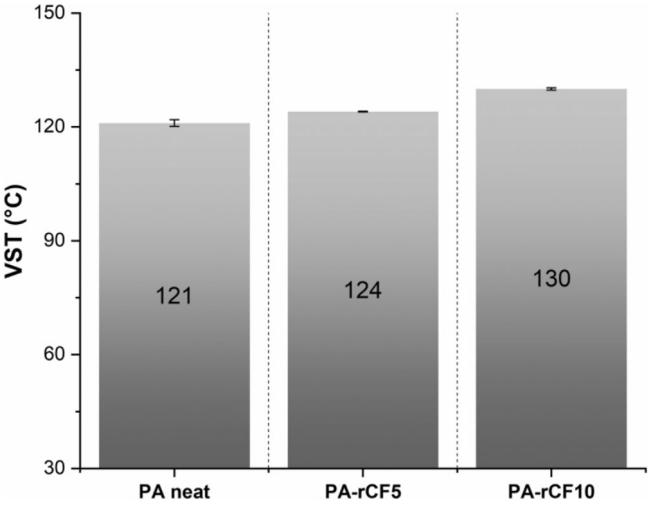

FIGURE 6 Vicat softening temperature (VST) test results of filaments.

FIGURE 7 Three-dimensionally printed shark fin antenna covers using polyamide (PA)-recycled milled carbon fiber (rCF) filaments.

3.2 | Three-dimensional printing: design, modeling, and fabrication of the automotive demonstrator

The shark fin antenna cover was chosen as a simple design to realize by 3D printing a semi-structural component for automotive applications. The selected demonstrator was produced with two different size scales and two different infill percentages (0% and 25%) to understand how the filament works during the print deposition (Figure 7). The 3D printed shark fin antenna cover seems to have a good shape and printing accuracy useful to verify the correct deposition of the self-produced filament and to understand if the set parameters were the correct ones for the printing process.

The hollow parts present some aesthetic defects near the bottom of the part probably due to mis-deposition of the composite material during the printing step (see the dotted areas in yellow in Figure 8). As it is possible to see from Figure 8, the length of these defects is around 60 mm for the PA-rCF10 replica and 81 mm for the PA-rCF5 replica, respectively.

The walls of these samples are not so rigid, but a little bit flexible, so that when the print head builds the wall, the motion of the print head can generate some vibrations that can cause defects while extruding. Instead, the antenna shark replicas with 25% infill are more rigid than the hollow ones, and their walls are reinforced by the infill itself. In this way, the problem observed in the hollow replicas does not occur, and no aesthetic defects can be found on the final 3D printed objects. These results suggest that it is more challenging to print big parts with hollow infill with this kind of filament. On the contrary,

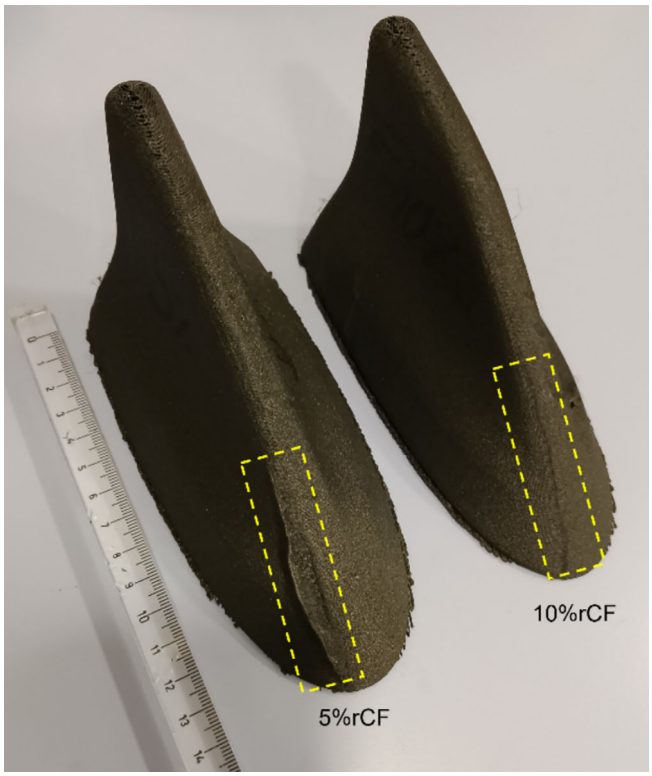

FIGURE 8 The hollow antenna shark fin with a bottom defect: On the left is the PA-rCF5 replica, and on the right is the PA-rCF10 replica.

the hollow infill is a good way to successfully print a 3D part, saving time and material.

Moreover, both replicas, with infill and hollow, present a defect at the top of the part, which is almost parallel to the building platform. This could cause material

failure while extruding it. For hollow replicas, this defect is almost 28 mm long for PA-rCF5 samples and 40 mm for PA-rCF10, as visible in Figure 9.

It is also possible to see this kind of defect on the 25% infill replicas, where the defect is 17 mm long for PA66 + 5%rCF and 19 mm for PA66 + 10%rCF, respectively as illustrated in Figure 10. This defect on the top of the antenna is higher in the hollow and bigger replicas and can be ascribed to the fact that the hollow replica is not structurally reinforced on the inner side, so that the defect is proportionally bigger.

Despite these few defects, the 3D printed demonstrators present a good level of resolution and dimensional accuracy. Further optimization of the process parameters could help to overcome this issue, leading to the realization of more detailed demonstrators for the automotive field.

3.3 | Characterization of 3D printed composites

3.3.1 | Thermogravimetric analysis

The results of TGA of the filament and 3D printed rCF-filled composites are listed in Table 5 and show that FFF processing has a negligible effect on the thermal stability of the material. A substantial difference between filament and printed samples is noted in the TG residue. The analysis on the FFF printed parts highlights higher rCFs content than that of the feed (nominal), supporting the uneven distribution of the filler material within the printed parts. Moreover, the further extrusion process due to 3D printing can cause fiber breakage and downsizing. Wang et al.[30] already analyzed this phenomenon, called fiber attrition, by comparing the fiber size

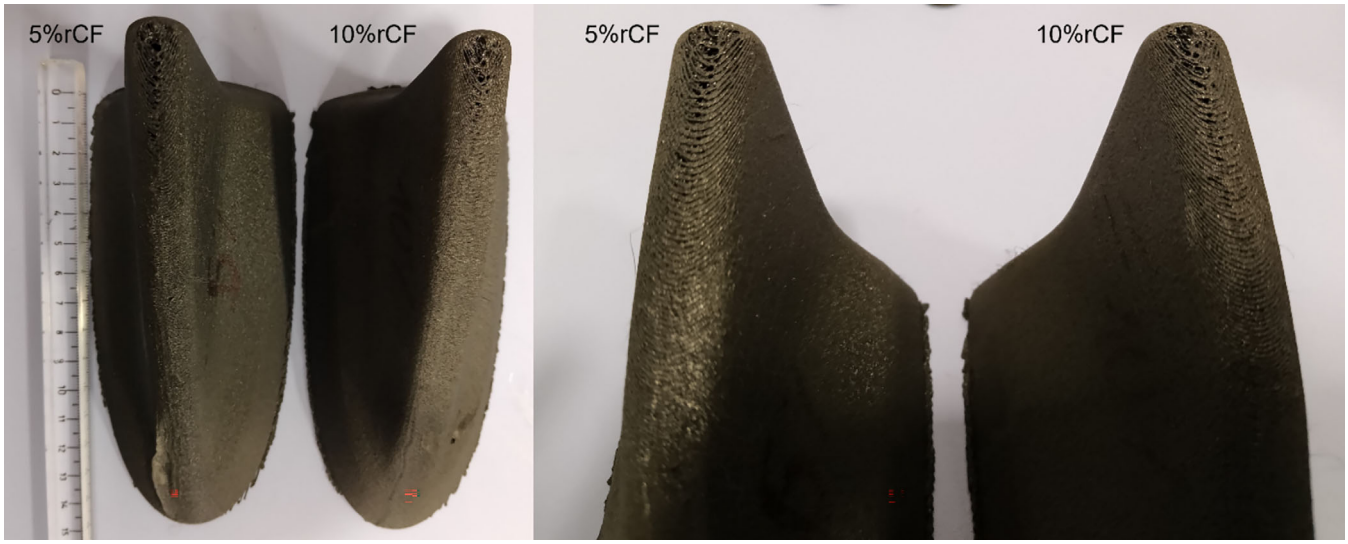

FIGURE 9 The hollow antenna shark fin with top defect: On the left PA-rCF5 replica, on the right PA-rCF10 replica.

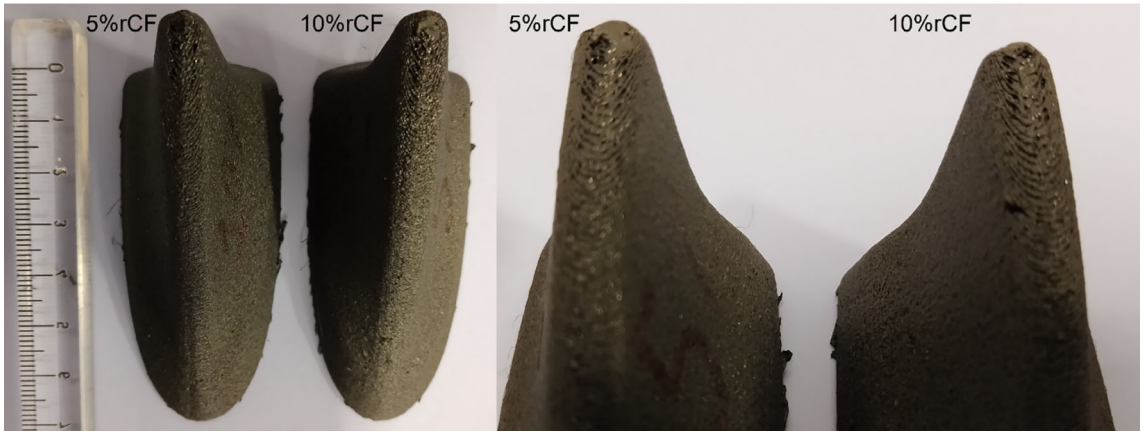

FIGURE 10 Top view of the 25% infill antenna shark fin: On the left is the PA-rCF5 replica, and on the right is the PA-rCF10 replica, respectively.

reduction in discontinuous fiber-reinforced thermoplastic composites prepared via material extrusion (filament) and FFF 3D printing. The authors noted that the reduction in average length (original average length of 100–150 μm) was more marked in the printed parts than filament, suggesting limit values of reinforcing fibers within 10 wt% (as those implemented in the present work) to mitigate significant reductions in mechanical properties while maintaining adequate printability of the material.

3.3.2 | Differential scanning calorimetry

Figure 11A,B display the DSC thermograms of filament and printed rCF-based composites (5 wt% rCFs and 10 wt % rCFs, respectively). The results are summarized and listed in Table 6. The 3D printing process does not alter the thermal characteristics of the material in terms of T_g, T_m, and T_c. A slight difference can be observed in the degree of crystallinity. The 3D printed samples show a slight increase in X_c in accordance with two possible reasons: (1) consecutive extrusion cycles (material extrusion for filament production +3D printing) can induce thermomechanical degradation of the material and therefore scission of the macromolecular chains. The tendency of the smaller chains to fit among the longer ones promotes the packing of these chains into crystalline domains, and therefore an increase in the degree of crystallinity is observed[31]; (2) the higher rCFs content in the printed specimens compared to the filament (detected by TGA) may be sufficient to enable heterogeneous nucleation mechanisms induced by the carbon filler, resulting in a decrease of the activation energy in the crystallization process.[32]

The thermal profile (TGA and DSC) of 3D printed PA-rCF composites is consistent with the performance typically required for automotive parts manufactured through injection molding. Engineering thermoplastic polymers and composites commonly used in automotive components are designed to withstand service temperatures ranging from 110 to 130°C, depending on exposure duration.[33] Additionally, the T_g values of the 3D printed material, which are critical indicators of the durability of automotive components under varying

TABLE 5 Results of thermogravimetric (TG) analysis on filament and printed composite specimens.

TGA results: filament versus printed samples				
Sample	**$T_{5\%}$ (°C)**	**$T_{10\%}$ (°C)**	**T_{deg} (°C)**	**rCFs residue at 800°C (%)**
PA-rCF5 (filament)	387	410	457	4.1
PA-rCF5 (printed)	382	410	458	7.7
PA-rCF10 (filament)	386	411	458	7.7
PA-rCF10 (printed)	379	409	456	11.0

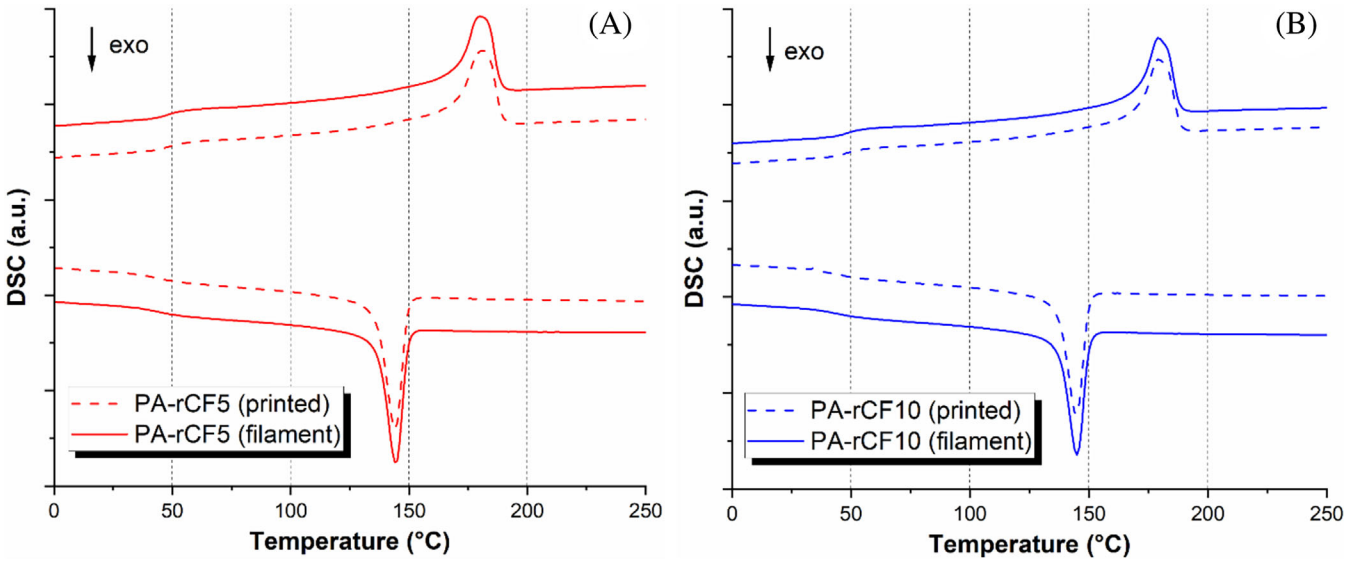

FIGURE 11 Differential scanning calorimetry thermograms comparison between filament and printed samples: (A) PA-rCF5 and (B) PA-rCF10. The heat flow (y-axis) is expressed in arbitrary units (a.u.) due to shifting of the curve baselines for better readability.

TABLE 6 Results of differential scanning calorimetry (DSC) measurements on filament and printed composite specimens.

DSC results: filament versus printed samples					
Sample	T_g (°C)	T_c (°C)	T_m (°C)	ΔH_m (J/g)	X_c (%)
PA-rCF5 (filament)	49	144	180	53.9	29
PA-rCF5 (printed)	50	144	181	54.6	30
PA-rCF10 (filament)	49	145	179	50.7	28
PA-rCF10 (printed)	51	145	179	51.2	29

climatic conditions and harsh environments, fall within the acceptable range for PA-based injection molded products used in automotive applications (40–50°C), as reported in the review by Kondo et al.[34]

3.3.3 | VST analysis

The effect of the 3D printing process on the VST is shown in Table 7. VST values of printed bars are lower than bulk composites processed by injection molding. The reason behind this observed decrease in VST is mainly attributable to the effect of voids and air pockets resulting from the layer-by-layer deposition. These defects, besides acting as mechanical weakness points, reduce the thermo-mechanical properties of the material (including the VST). Similar results were reported by Dul et al.,[35] who investigated the effect of short carbon fibers on the thermo-mechanical properties of 3D-printed PA composite parts, and by Rigotti et al.[36] studying the printability and properties of recycled HDPE-fiber glass composites tailored for FFF technology. The drop in VST found in this work (about 10°C between injection molded and 3D printed objects) can, however, be considered still acceptable for the proposed application in the automotive industry. Generally, the service temperature range of common plastics used for producing automotive commodities can reach a threshold value up to 120°C.[37]

TABLE 7 Vicat softening temperature (VST) comparison between injection molded and printed composite samples.

VST results: injection molded versus printed samples	
Sample	**VST (°C)**
PA-rCF5 (injection molded)	124.0 ± 0.1
PA-rCF5 (printed)	117.0 ± 0.4
PA-rCF10 (filament)	130.0 ± 0.3
PA-rCF10 (printed)	120.0 ± 1.3

TABLE 8 Porosity analysis on 3D printed composite specimens.

Porosity evaluation on printed samples			
Sample	ρ_{fil} (g/cm^3)	ρ_{3D} (g/cm^3)	P (%)
PA-rCF5	1.15 ± 0.02	1.11 ± 0.01	3.48 ± 0.03
PA-rCF10	1.16 ± 0.01	1.14 ± 0.02	1.72 ± 0.03

3.3.4 | Porosity evaluation on printed samples

The porosity results of the printed specimens loaded with 5 and 10 wt% of rCFs are reported in Table 8. The low void content in the printed parts (less than 4%) indicates a good quality printing process considering that other studies have shown that the inclusion of short fibers induces higher porosity in FFF fabricated samples, which usually range between 13% and 17%.[38] Interestingly, it is noted that as the rCFs dosage increases, the porosity progressively decreases, ranging from 3.48% in the PA-rCF5 sample to 1.72% in the PA-rCF10 sample. These results suggest that the addition of conductive fibers, like rCFs used in the present work, would enhance the heat transfer between the printed filaments. Then, the extruded filament and the surrounding material reach a high enough temperature and keep it for long enough to enable bonding between adjacent layers.[39]

3.3.5 | Scanning electron microscopy

The morphology of the printed parts obtained by FFF was also investigated by means of SEM analysis. Figure 12 reports micrographs at different magnifications, 500× (A,C) and 1000× (B,D), for the PA-rCF5 and PA-rCF10 specimens (fracture surfaces).

Looking at the surface fractures of the PA-rCF5 and PA-rCF10 samples, the samples loaded with different amounts of recycled carbon fibers show a completely different microstructure.

SEM micrographs of the PA-rCF5 samples evidence voids that can be due to the presence of bubbles of air

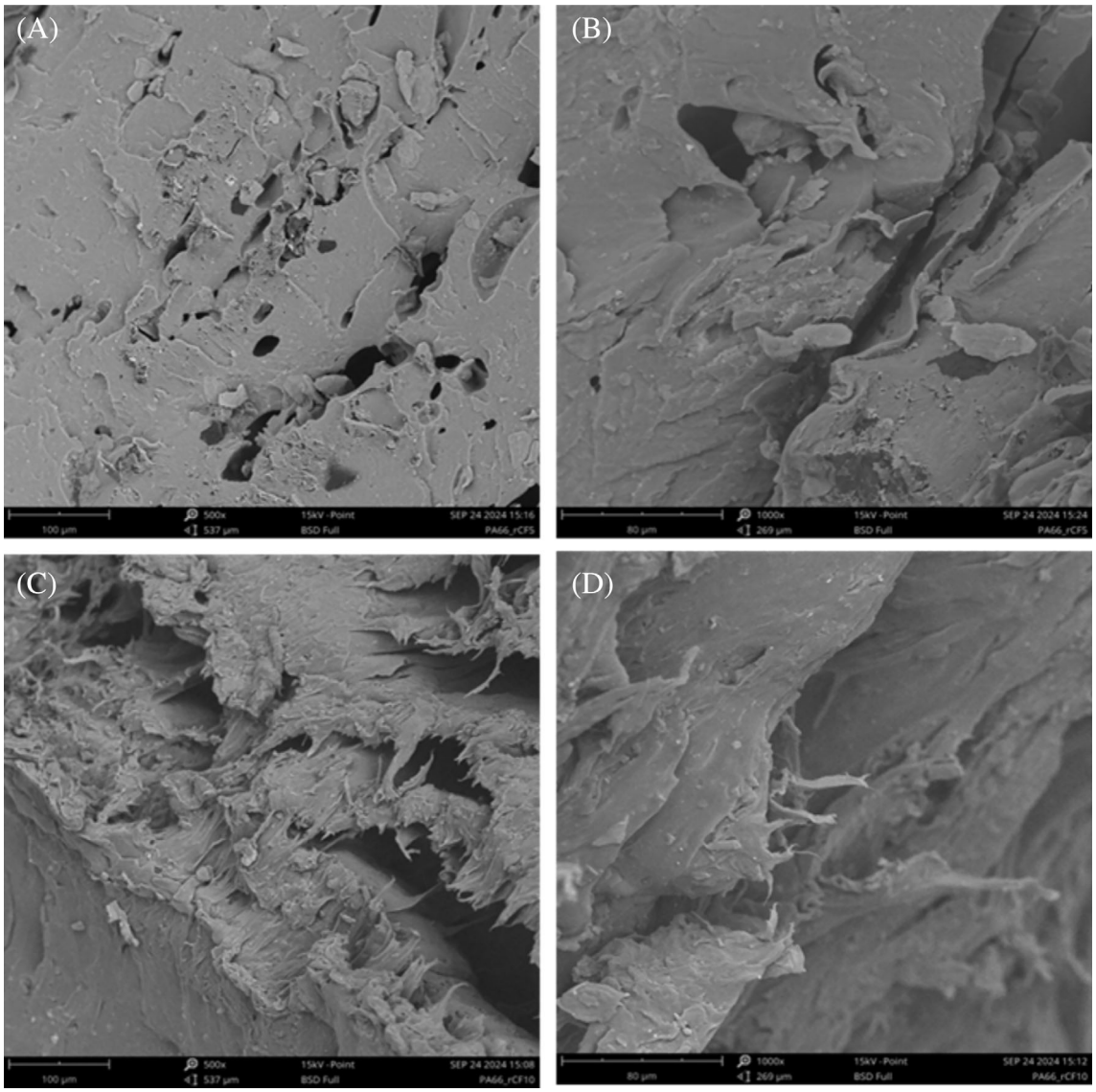

FIGURE 12 Scanning electron microscopy micrographs at different magnifications, 500× and 1000×, of PA-rCF5 replica (A,B) and of PA-rCF10 replica (C,D), respectively.

probably formed during the printing process. It can also be noted that the voids have different lengths varying from 10 up to 100 micrometers. On the contrary, the PA composites filled with 10 wt% of rCF seem to have a bulk morphology where it is evident the stratification of the material and, in some regions, the poor adhesion among successive polymeric layers mainly due to the printing process. On both samples, rCFs dispersed within the PA66 matrix are not so evident because of the low amount of fibers present within the composite and probably because of several stresses occurring during the preparation of the filament and the printing process that can significantly affect their length. Furthermore, no rCFs agglomerations are detected.

4 | CONCLUSIONS

The focus of this work was exploring the thermal, rheological, and printability characteristics of polyamide matrix filaments for FFF 3D printing loaded with rCFs. After thermo-rheological characterization of the filaments filled with different content of fibers (5 and 10 wt %), the printing quality was tested through the additive fabrication of technological automotive demonstrators, specifically car shark fin antennas. This research demonstrated that rCFs can be a good circular and eco-friendly candidate to be used as reinforcement for 3D printed thermoplastic composites for mitigating the solid waste issue while increasing the added value of the recycled polymers. The major outcomes are listed below:

The thermal analysis (TG and DSC) conducted on filament specimens revealed that the inclusion of rCFs did not significantly alter the properties of the neat PA matrix. However, a slight increase in the T_m and T_c was observed, likely due to the heterogeneous nucleation effect and the blockage of macromolecular movement caused by the carbon filler. The fibers had a more noticeable impact on the rheology and thermo-mechanical stability of the composites, with a progressive increase in melt viscosity and VST as the rCF content rose. These thermo-rheological results were useful for optimizing the selection of printing parameters. After refining these parameters, car shark fin antenna prototypes were successfully printed using both PA-rCF filaments. The 3D printed parts demonstrated an adequate level of resolution and dimensional accuracy. Further process optimization could address some structural defects and enable the creation of more detailed automotive prototypes. Additionally, future research could explore how rCF-composites affect electromagnetic transmission behavior, considering the dielectric and conductivity properties of carbon fibers. Thermo-mechanical analysis of the printed materials did not show significant changes in thermal stability or transition temperatures (T_m, T_c, and T_g). Although the printed samples exhibited minimal porosity (<4%), indicating a high-quality 3D printing process, the parts showed a slight reduction of about 10°C in VST, which remained within acceptable levels for automotive applications. Scanning electron microscopy (SEM) images revealed only minor defects such as air pockets and delamination, but no fiber clustering or significant inter-filament gaps.

Continuing from the results achieved, the next logical research efforts would be to refine the additive processability of the composite filaments to overcome defects and printing issues found in the produced prototypes. This aspect, combined with the implementation of targeted analyses on the printed component (e.g., electromagnetic signal transmission measurements for car shark fin antennas) should promote the advancement of FFF mass production since the associated costs and material consumption can be significantly reduced.

ACKNOWLEDGMENTS

This study was carried out within the Made in Italy–Circular and Sustainable (MICS) Extended Partnership and received funding from the European Union Next-Generation EU (PIANO NAZIONALE DI RIPRESA E RESILIENZA (PNRR)–MISSIONE 4 COMPONENTE 2, INVESTIMENTO 1.3–D.D. 1551.11-10-2022, PE00000004). This manuscript reflects only the authors' views and opinions; neither the European Union nor the European Commission can be considered responsible for them. The authors would also like to thank Christian Scopinich (Carbon Task Srl) for providing recycled milled carbon fibers used in the research activity. Open access publishing facilitated by Universita degli Studi di Roma La Sapienza, as part of the Wiley - CRUI-CARE agreement.

DATA AVAILABILITY STATEMENT

The data that support the findings of this study are available from the corresponding author upon reasonable request.

ORCID

Matteo Sambucci https://orcid.org/0000-0002-0974-2129
Giovanna Colucci https://orcid.org/0000-0002-8178-6644
Irene Bavasso https://orcid.org/0000-0003-2736-4915
Marco Valente https://orcid.org/0000-0002-6298-3693
Massimo Messori https://orcid.org/0000-0003-3598-4241

REFERENCES

1. Rett JP, Traore YL, Ho EA. Sustainable materials for fused deposition modeling 3D printing applications. *Adv Eng Mater*. 2021;23(7):2001472. doi:10.1002/adem.202001472
2. Olawumi MA, Oladapo BI, Olugbade TO. Evaluating the impact of recycling on polymer of 3D printing for energy and material sustainability. *Resour Conserv Recycl*. 2024;209:107769. doi:10.1016/j.resconrec.2024.107769
3. Omar NWY, Shuaib NA, Hadi MHJA, Azmi AI, Misbah MN. Mechanical and physical properties of recycled-carbon-fiber-reinforced Polylactide fused deposition modelling filament. *Materials*. 2022;15(1):190. doi:10.3390/ma15010190
4. Karimi A, Rahmatabadi D, Baghani M. Various FDM mechanisms used in the fabrication of continuous-fiber reinforced composites: a review. *Polymers*. 2024;16(6):831. doi:10.3390/polym16060831
5. Milosevic M, Stoof D, Pickering KL. Characterizing the mechanical properties of fused deposition modelling natural fiber recycled polypropylene composites. *J Compos Sci*. 2017;1:7. doi:10.3390/jcs1010007
6. Mishra VM, Negi S, Kar S. FDM-based additive manufacturing of recycled thermoplastics and associated composites. *J Mater Cycles Waste Manag*. 2023;25(2):758-784. doi:10.1007/s10163-022-01588-2
7. Su N, Pierce RS, Rudd C, Liu X. Comprehensive investigation of reclaimed carbon fibre reinforced polyamide (rCF/PA) filaments and FDM printed composites. *Compos Part B: Eng*. 2022;233:109646. doi:10.1016/j.compositesb.2022.109646
8. Seok W, Jeon E, Kim Y. Effects of annealing for strength enhancement of FDM 3D-printed ABS reinforced with recycled carbon fiber. *Polymers*. 2023;15:3110. doi:10.3390/polym15143110
9. Ateeq M, Shafique M, Azam A, Rafiq M. A review of 3D printing of the recycled carbon fiber reinforced polymer composites: processing, potential, and perspectives. *J Mater Res Technol*. 2023;26:2291-2309. doi:10.1016/j.jmrt.2023.07.171
10. Liu W, Huang H, Zhu L, Liu Z. Integrating carbon fiber reclamation and additive manufacturing for recycling CFRP waste. *Compos Part B: Eng*. 2021;215:108808. doi:10.1016/j.compositesb.2021.108808
11. Katalagarianakis A, van de Voorde B, Pien N, et al. The effect of carbon fiber content on physico-mechanical properties of

recycled poly(ethylene terephthalate) composites additively manufactured with fused filament fabrication. *Addit Manuf*. 2022;60:103246. doi:10.1016/j.addma.2022.103246

12. BMW Group. Accessed August. 2024 https://www.press.bmwgroup.com/global/photo/detail/P90125888/bmw-i-production-cfrp-wackersdorf-carbon-fiber-recycling-material-for-the-use-in-the-bmw-i3-e-g-the
13. Sanko Gosei. Accessed August 8. 2024 https://sanko-gosei.co.uk/world-class-moulding-and-tooling/
14. Visa Cash App RB. Accessed August 8. 2024 https://www.visacashapprb.com/en/partnership-hera-group/
15. Valente M, Sambucci M, Rossitti I, et al. Carbon-fiber-recycling strategies: a secondary waste stream used for PA6,6 thermoplastic composite applications. *Materials*. 2023;16:5436. doi:10.3390/ma16155436
16. Valente M, Rossitti I, Biblioteca I, Sambucci M. Thermoplastic composite materials approach for more circular components: from monomer to in situ polymerization, a review. *J Compos Sci*. 2022;6:132. doi:10.3390/jcs6050132
17. Lupone F, Tirillò J, Sarasini F, Badini C, Sergi C. 3D printing of low-filled basalt PA12 and PP filaments for automotive components. *J Compos Sci*. 2023;7:367. doi:10.3390/jcs7090367
18. Liao G, Li Z, Luan C, Wang Z, Yao X, Fu J. Additive manufacturing of polyamide 66: effect of process parameters on crystallinity and mechanical properties. *J Mater Eng Perform*. 2022;31(1):191-200. doi:10.1007/s11665-021-06149-6
19. Xiao X, Chevali VS, Song P, He D, Wang H. Polylactide/hemp hurd biocomposites as sustainable 3D printing feedstock. *Compos Sci Technol*. 2019;184:107887. doi:10.1016/j.compscitech.2019.107887
20. Zheng Z, Yao JL, Yao Q. Thermal degradation of polyamide 66 and its model compound. *Polym Degrad Stab*. 2024;228:110909. doi:10.1016/j.polymdegradstab.2024.110909
21. Giani N, Mazzocchetti L, Benelli T, Picchioni F, Giorgini L. Towards sustainability in 3D printing of thermoplastic composites: evaluation of recycled carbon fibers as reinforcing agent for FDM filament production and 3D printing. *Compos A: Appl Sci Manuf*. 2022;159:107002. doi:10.1016/j.compositesa.2022.107002
22. Kada D, Koubaa A, Tabak G, Migneault S, Garnier B, Boudenne A. Tensile properties, thermal conductivity, and thermal stability of short carbon fiber reinforced polypropylene composites. *Polym Compos*. 2018;39(S2):E664-E670. doi:10.1002/pc.24093
23. Sridhara PK, Vilaseca F. Assessment of fiber orientation on the mechanical properties of PA6/cellulose composite. *Appl Sci*. 2020;10:5565. doi:10.3390/app10165565
24. Qiao L, Yan X, Tan H, et al. Mechanical properties, melting and crystallization behaviors, and morphology of carbon nanotubes/continuous carbon fiber reinforced polyethylene terephthalate composites. *Polymers*. 2022;14:2892. doi:10.3390/polym14142892
25. Wang S, Capoen L, D'hooge DR, Cardon L. Can the melt flow index be used to predict the success of fused deposition modelling of commercial poly (lactic acid) filaments into 3D printed materials? *Plast Rubber Compos*. 2018;47(1):9-16. doi:10.1080/14658011.2017.1397308
26. Doronin F, Rudakova A, Rytikov G, Nazarov V. Simple determination of the melt flow index of composite polymer filaments used in material extrusion additive manufacturing. *Coatings*. 2023;13:1592. doi:10.3390/coatings13091592
27. Li X, He J, Hu Z, et al. High strength carbon-fiber reinforced polyamide 6 composites additively manufactured by screw-based extrusion. *Compos Sci Technol*. 2022;229:109707. doi:10.1016/j.compscitech.2022.109707
28. Tait M, Pegoretti A, Dorigato A, Kalaitzidou K. The effect of filler type and content and the manufacturing process on the performance of multifunctional carbon/poly-lactide composites. *Carbon*. 2011;49(13):4280-4290. doi:10.1016/j.carbon.2011.06.009
29. Zhang L, Han E, Wu Y, Wang X, Wu D. Surface decoration of short-cut polyimide fibers with multi-walled carbon nanotubes and their application for reinforcement of lightweight PC/ABS composites. *Appl Surf Sci*. 2018;442:124-137. doi:10.1016/j.apsusc.2018.02.129
30. Wang Z, Fang Z, Xie Z, Smith DE. A review on microstructural formations of discontinuous fiber-reinforced polymer composites prepared via material extrusion additive manufacturing: fiber orientation, fiber attrition, and micro-voids distribution. *Polymers*. 2022;14:4941. doi:10.3390/polym14224941
31. Tsai H-H, Wu S-J, Wu Y-D, Hong W-Z. Feasibility study on the fused filaments of injection-molding-grade poly(ethylene terephthalate) for 3D printing. *Polymers*. 2022;14:2276. doi:10.3390/polym14112276
32. Tian H, Zhang S, Ge X, Xiang A. Crystallization behaviors and mechanical properties of carbon fiber-reinforced polypropylene composites. *J Therm Anal Calorim*. 2017;128:1495-1504. doi:10.1007/s10973-016-5996-3
33. Glasscock D, Atolino W, Kozielski G, Martens M. High performance polyamides fulfill demanding requirements for automotive thermal management components. *DuPont Eng Polym*. 2008;1-9.
34. Kondo MY, Montagna LS, Morgado GFDM, et al. Recent advances in the use of polyamide-based materials for the automotive industry. *Polimeros*. 2022;32(2):e2022023. doi:10.1590/0104-1428.20220042
35. Dul S, Fambri L, Pegoretti A. High-performance polyamide/carbon fiber composites for fused filament fabrication: mechanical and functional performances. *J Mater Eng Perform*. 2021;30:5066-5085. doi:10.1007/s11665-021-05635-1
36. Daniele R, Armoni D, Dul S, Alessandro P. From nautical waste to additive manufacturing: sustainable recycling of high-density polyethylene for 3D printing applications. *J Compos Sci*. 2023;7:320. doi:10.3390/jcs7080320
37. Bernreitner K, Hammerschmid K. Motivations for tailoring of properties. *Polypropylene: An AZ Reference*. Vol 1. Springer; 1998:148.
38. Gómez-Ortega A, Piedra S, Mondragón-Rodríguez GC, Camacho N. Dependence of the mechanical properties of nylon-carbon fiber composite on the FDM printing parameters. *Compos Part A: Appl Sci Manuf*. 2024;186:108419. doi:10.1016/j.compositesa.2024.108419
39. Blok LG, Longana ML, Yu H, Woods BKS. An investigation into 3D printing of fibre reinforced thermoplastic composites. *Addit Manuf*. 2018;22:176-186. doi:10.1016/j.addma.2018.04.039

How to cite this article: Sambucci M, Colucci G, Fontana L, et al. Recycled milled carbon fibers in fused filament fabrication of composite filaments: Thermophysical analysis and 3D printability assessment for automotive parts manufacturing. *Polym Compos*. 2025;46(14):12950-12965. doi:10.1002/pc.29909